Top Catal (2010) 53:1311–1318
DOI 10.1007/s11244-010-9589-2

ORIGINAL PAPER

Synthesis of Pure VSH-2 in Large Quantities and Its Characterization

Shuvo Jit Datta · Kyung Byung Yoon

Published online: 7 October 2010

Abstract A method to produce pure VSH-2 in large quantities (~20 g) was developed. The reagents were silica sol, V_2O_5, H_2SO_4, CsOH, and ethanol. Despite the fact that V_2O_5 was used as the vanadium source the oxidation states of most of the vanadium atoms in the produced VSH-2 were 4+, indicating that ethanol acts as a reducing agent. The crystals adopted individual octahedral shapes or aggregated states depending on the gel composition. The total surface area of the pristine VSH-2 with the general formula of $Cs_2(VO)(Si_6O_{14})\cdot 3H_2O$ was only 40 m^2/g, indicating that the pores are blocked by the large Cs^+ ions. The surface area increased to 149 m^2/g upon exchanging Cs^+ with Na^+. Analyses of the diffuse reflectance UV–Vis spectra of M^{n+}–VSH-2 (M^{n+} = Cs^+, Na^+, Ca^{2+}, and Pb^{2+}) revealed that the 215, 250, and 313 nm bands arise due to the V^{4+} to O^{2-} metal-to-ligand charge transfer (MLCT) and the 437, 590, and 914 nm bands arise due to the d–d transition of V^{4+}. This reveals an unprecedented interesting situation that in dehydrated VSH-2 the framework oxide plays the role of both acceptor to V^{4+} and donor to M^{n+}. The measured atomic magnetic moment (μ) was 1.64 BM, indicating that most of the V atoms exist in V^{4+}. The ESR spectrum of VSH-2 showed a strong signal due to V^{4+} with the g value of 1.959 with ΔH_{pp} value of 168 G. The Raman spectra of M^{n+}–VSH-2 revealed the existence of strong V=O stretching at 960 cm^{-1}, and other weak peaks. The V=O stretching band shifted to a higher energy region upon increasing the Sanderson's electronegativity of M^{n+}. The thermogravimetric (TGA) analysis showed that VSH-2 is thermally stable up to 550 °C and above which the oxidation of V^{4+} occurs.

Keywords VSH-2 · Large scale synthesis · Ethanol as the reducing agent · Characterization · V^{4+} to O^{2-} charge transfer

1 Introduction

Microporous vanadosilicate molecular sieves have great potential to be used as useful catalysts for various reactions due to its high thermal stability and, in particular, due to the fact that V, as a transition metal, can adopt several different oxidation states [1–11]. Among these, the V=O group containing open framework vanadosilicates have great potential to be used as oxidation catalysts [1–5]. In this respect, the catalytic activities of VSH-*n* series molecular sieves which were prepared and characterized by Jacobson and the co-workers [1, 2] should be investigated. Along with this, their unique physical properties should be elucidated. However, the VSH-*n* series molecular sieves have been synthesized only in small scales aimed for structure determinations and they have often been produced with other impurities [1, 2]. As a result, their catalytic properties and various physical properties have not yet been elucidated. The same arguments also apply to VSH-2 [1, 2].

The structure of VSH-2 is closely related to that of pentagonite, a natural mineral, whose structure and composition were determined by Staples [4] and Evans [5], respectively, in 1973. The chemical compositions of pentagonite and VSH-2 are $Ca(VO)(Si_6O_{14})\cdot 4H_2O$ [4, 5] and $Cs_2(VO)(Si_6O_{14})\cdot 3H_2O$, [1] respectively. The space group of VSH-2 is *Cmca*. VSH-2 is constructed by interconnecting silicate sheets with V=O units. Each silicate sheet is composed of six

S. J. Datta · K. B. Yoon (✉)
Department of Chemistry, Center for Nano Materials, Sogang University, Seoul 121-742, Korea
e-mail: yoonkb@sogang.ac.kr

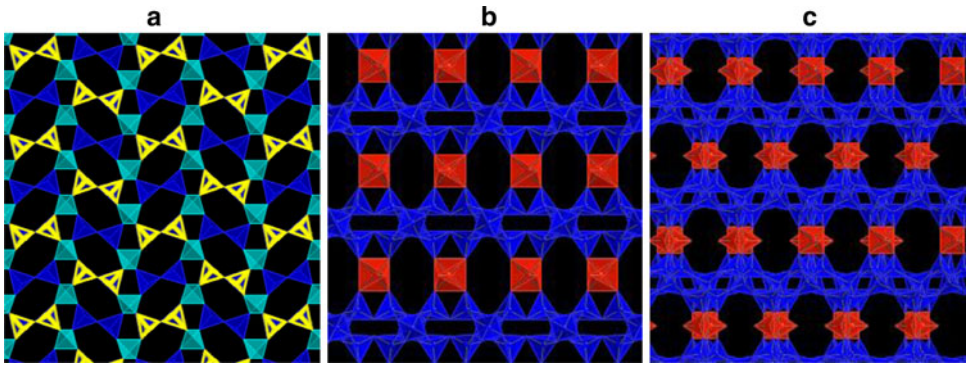

Fig. 1 Polyhedral view of VSH-2. **a** The top view of a single silicate sheet showing the formation of six and four membered rings by interconnecting four Q3 tetrahedral silicate (*yellow* and *blue*) and two Q4 tetrahedral silicate units (*cyan*). Two pointed up Q3 units (*yellow*) form a dimer and two pointed down Q3 units (*blue*) form a dimer and they are interconnected by Q4 units (*cyan*) forming four and six membered rings. **b** The view along the (010) direction showing the interconnection of the silicate sheets by the oxovanadyl square planar units forming eight member rings. **c** The view along the (011) direction showing the formation of eight membered ring with the opening of 3.0 × 3.5 Å by interconnection of the silicate sheets with the oxovanadyl square planar units

tetrahedral silicate units consisting of four Q3 tetrahedral silicate units and two Q4 tetrahedral silicate units. The Q3 tetrahedral silicate unit denotes the silicate unit which is connected to three other tetrahedral silicates in the same sheet and to an oxovanadate (O=V) unit, which interconnects the sheet to the neighbouring sheet. The Q4 tetrahedral silicate unit denotes the silicate unit that interconnects four Q3 tetrahedral silicate units within a sheet. Among the four Q3 tetrahedral silicate units, two of them form a dimer with the vertices pointing up to be connected to a O=V unit and two of them form a dimer with the vertices pointing down to be connected to a O=V unit. The pointed-up Q3 silicate dimer and the pointed-down Q3 silicate dimer are interconnected by the two single Q4 silicate units in such a way that six and four-membered rings form (Fig. 1a). The neighbouring two silicate sheets are interconnected by oxovanadium (O=V) units. Thus, each oxovanadium (O=V) unit interconnects the pointed-down Q3 silicate dimer in the upper layer and the pointed-up Q3 silicate dimer in the bottom layer, forming a square-planar shaped oxovanadate unit. Accordingly, there are eight-membered rings when viewed along the (010) direction (Fig. 1b) and eight-membered rings when viewed along the (011) direction (Fig. 1c). The free aperture of each eight membered ring is 3.0 × 3.5 Å. The directions of the O=V groups are placed normal to the (011) direction. However, their orientations are disordered. Accordingly, in the eight-membered rings viewed along the (011) directions, there are three types of eight-membered rings having zero, one, or two O=V groups pointing to the center. In any case, although the ring sizes are rather small, the O=V groups are available in the eight-membered rings. Therefore, these O=V groups, together with the ability of the vanadium ion to change its oxidation state, bear great potential to be applied for various catalytic reactions. However, there have been no methods to synthesize pure VSH-2 in large scales.

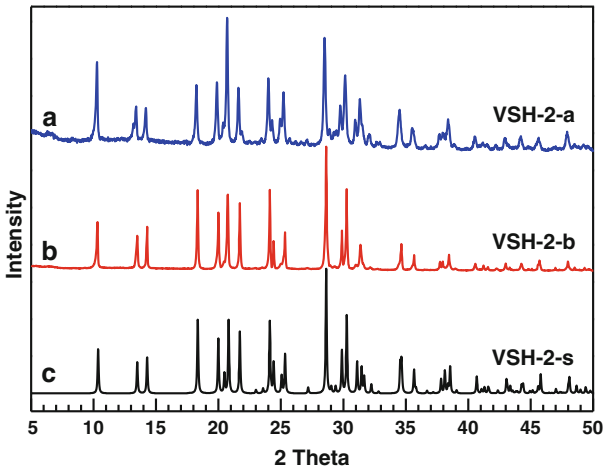

Fig. 2 Comparison of the X-ray powder diffraction patterns of VSH-2-a (**a**) and VSH-2-b (**b**) simulated pattern derived from the crystal structure reported by Jacobson and the coworkers (VSH-2-s) [1] (**c**)

Stemming from our recent achievement on the synthesis of ideal AM-6 in large quantities [9], we have successfully developed a hydrothermal method to produce pure VSH-2 in large quantities (∼20 g). Herein we report the synthetic procedure for VSH-2, Raman and diffuse-reflectance UV–Vis spectra of various ion-exchanged forms, and other useful information regarding VSH-2.

2 Experimental Section

2.1 Materials

Silica sol (40% aqueous of colloidal silica, Ludox HS-40, Aldrich), vanadium oxide (V_2O_5, 99%, Aldrich), sulfuric acid (H_2SO_4, 95%, Duksan), cesium hydroxide monohydrate

(CsOH, Aldrich), and ethanol (EtOH, 95%, SK) were purchased and used without further purification.

2.2 Procedure

A gel consisting of Ludox HS-40, V_2O_5, H_2SO_4, CsOH, EtOH, and DDW (distilled deionized water) was prepared, where the molar ratio of the gel in terms of SiO_2:V_2O_5:H_2SO_4:Cs_2O:EtOH:H_2O was 1:0.18:0.75:1.01:1.77:50. The gel was prepared as follows. (I) Preparation of the Si source solution: A CsOH solution (12.6 g CsOH and 20 g of DDW) was added into the 5.5 g of Ludox HS-40, and the mixture was stirred vigorously. (II) Preparation of the V source solutions: V solution A: H_2SO_4 (2.85 g) was added into a 25-mL round bottomed flask charged with DDW (10 g). V_2O_5 (1.25 g) and EtOH (3 g) were sequentially added into the flask. The heterogeneous mixture was refluxed for 1 h, during which the yellow V_2O_5 powder dissolved completely into the solution, and the solution turned ink blue. V solution B: A smaller amount of H_2SO_4 (2.45 g), instead of 2.85 g in solution A, was added into a 25-mL round bottomed flask charged with DDW (10 g). The amounts of other reactants V_2O_5 (1.25 g) and EtOH (3 g) that were sequentially added into the flask were the same as those of V solution A. The V solution B also turned ink blue during the course of stirring for 1 h. The V solutions were cooled to room temperature and subsequently added into the Si source solution in a drop wise manner. After aging the mixture for 12 h at room temperature, the gel was transferred into a 50-mL Teflon-lined autoclave, and placed in a preheated oven at 220 °C for 1 day under a static condition. The precipitated crystals were collected, washed, dried at 100 °C for 1 h, and analyzed by X-ray powder diffraction.

2.3 Instrumentation

Scanning electron microscopy (SEM) images were obtained using a field-emission scanning electron microscope (Hitachi S-4300) operating at an acceleration voltage of 20 kV. Elemental analyses of the samples were carried out by analyzing the energy-dispersive X-ray (EDX) spectra of the samples using a Horiba EMAX 6853-H EDX spectrometer. Transmission electron microscopy (TEM) images were collected on a JEOL JEM 4010 microscope. Raman spectra of the samples were recorded on a homemade setup equipped with an Ar^+ ion laser (Spectra-Physics Stabilite 2017) as an excitation beam source, a spectrometer (Horiba Jobin Yvon TRIAX 550), and a CCD detector (Horiba Jobin Yvon Symphony) cooled at −196 °C. The wavelength of the excitation beam was 514.5 nm. Diffuse-reflectance UV–Vis spectra of the samples were recorded on a Varian Cary 5000 UV–Vis–NIR spectrophotometer equipped with an integrating sphere. Barium sulfate was used as the reference. The diffuse reflectance spectra were converted into the Kubelka–Munk (K–M) formalism. Zero-field cooled (ZFC) susceptibility measurements of VSH-2 crystals were conducted from 4 to 300 K in a magnetic field of 5000 G on a SQUID magnetometer (MPMS5) placed at the Korea Basic Science Institute located in Korea University. Powder X-ray diffraction (XRD) patterns were obtained using a Rigaku D/MAX-2500/pc diffractometer. Thermogravimetric (TGA) analyses of the samples with air as the eluting gas were carried out on a TA Instruments (Thermal Analysis 2050). The temperature was increased from room temperature to 800 °C with the rate of 10 °C/min. The Brunauer–Emmett–Teller (BET) surface areas were obtained from N_2 adsorption at 77 K using a Quantachrome AUTOSORB-1. The samples were evacuated under a vacuum (3×10^{-5} Torr) at 300 °C. Electron spin resonance (ESR) spectra were measured at room temperature on a Bruker EMX 300 electron spin resonance spectrometer at the Korea Atomic Energy Research Institute.

3 Results and Discussion

3.1 X-Ray Diffraction Patterns

As described in the experimental section (vide supra) we prepared two gels with two different amounts of H_2SO_4. Thus the mole ratios of the two gels in terms of SiO_2:V_2O_5:H_2SO_4:Cs_2O:EtOH:H_2O were 1:0.18:0.75:1.01:1.77:50 and 1:0.18:0.65:1.01:1.77:50, respectively. Both gels produced pale green powders at the bottoms of the reactors after reaction at 220 °C for 1 day. The X-ray powder diffraction patterns of filtered and subsequently washed powders gave diffraction patterns which matched very well with the simulated powder diffraction pattern of VSH-2 (VSH-2-s), which was derived from the crystal structure reported by Jacobson and coworkers (Fig. 2) [1, 2]. This result indicates that the produced pale green powders from the above gels are pure VSH-2 crystals. Thus, our synthetic procedures produce pure VSH-2 crystals, unlike the procedure reported by Jacobson and co-workers [1, 2]. Hereafter we designate the VSH-2 crystals synthesized from the gel with the higher amount of H_2SO_4, in other words from the more acidic gel, as VSH-2-a and the VSH-2 crystals synthesized from the gel with the lower amount of H_2SO_4, in other words from the more basic gel, as VSH-2-b. We found that the procedure is easily scalable for the production of 20 g of VSH-2, demonstrating that our procedure is also highly effective for the production of larger amounts of pure VSH-2.

Jacobson and the co-workers used vanadyl sulfate $VOSO_4$ as the source of V, [1, 2] which is about five times more expensive than V_2O_5. Despite the fact that V_2O_5 is

used as the vanadium source, the oxidation states of most of the V atoms in the produced VSH-2 were 4+ (*vide infra*). In this respect, coupled with the fact that this method does not produce impurities, this method is also very useful in terms of the economic point of view.

3.2 Scanning Electron Microscope (SEM) Images

The SEM images of VSH-2-a and VSH-2-b crystals revealed that VSH-2-a crystals adopt typical octahedral shapes with the average size ~15 μm (Fig. 3a), while VSH-2-b crystals exist in the cluster forms (Fig. 3b). This result shows that the pH of the gel sensitively affects the morphology of the VSH-2 crystals. In both cases, the surfaces of the crystals were smooth. When the PH of the gel was further increased or when the amount of H_2SO_4 was further decreased, quartz was formed simultaneously.

3.3 High-Resolution Transmission Electron Microscopy (HR-TEM) Image

The HR-TEM image of VSH-2 viewed along the (011) direction is shown in Fig. 4 together with their structure viewed in the same direction and the fast Fourier-transform (FFT) image in the insets. The white dots indicate the small pores. Due to the beam damages, clearer images were difficult to obtain.

3.4 N_2 Adsorption Isotherms

The measured N_2 adsorption isotherms of Na^+–VSH-2-a and Cs^+–VSH-2-a with the relative pressure (p/p_o) between 0.0 and 1.0 are shown in Fig. 5. In the case of Na^+–VSH-2-a, about one third of the total adsorbed amounts were adsorbed when $p/p_o < 0.1$ and the rest of the amount were adsorbed when $p/p_o > 0.9$. The sudden substantial increase in the adsorbed amount at the relatively high pressure indicates that there are very small pores which are accessible only at high relative pressures. The total surface areas of

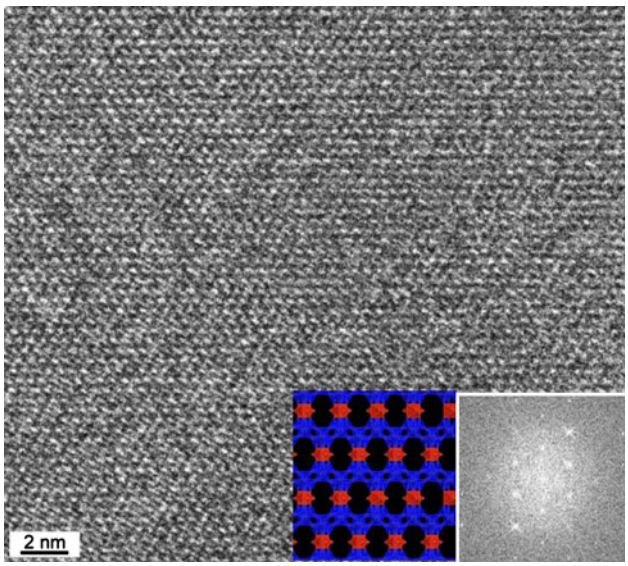

Fig. 4 HR-TEM image of VSH-2-a along the (011) direction and the corresponding polyhedral view and FFT image in the insets, respectively

Cs^+–VSH-2-a and Na^+–VSH-2-a were 40 and 149 m^2/g, respectively. The very small surface area of Cs^+–VSH-2-a indicates that most of the pores are blocked by the large Cs^+ cations.

3.5 Diffuse Reflectance UV–Vis Spectra

The diffuse reflectance spectra of M^{n+}–VSH-2-a, where $M^{n+} = Cs^+$, Na^+, Ca^{2+}, and Pb^{2+}, are shown in Fig. 6 for the cases of hydrated (a and b) and dehydrated (c and d) states in the spectral regions between 200 and 1500 nm (a and c) and between 200 and 400 nm (b and d). In the hydrated states, the diffuse reflectance spectra of M^{n+}–VSH-2-a are nearly identical having absorption maximums (λ_{max}) at 215 (0.926), 250 (0.349), 313 (0.016), 437 (0.007), 590 (0.010), 914 nm (0.040), respectively, with the relative intensities shown in the parentheses. In the case of dehydrated state,

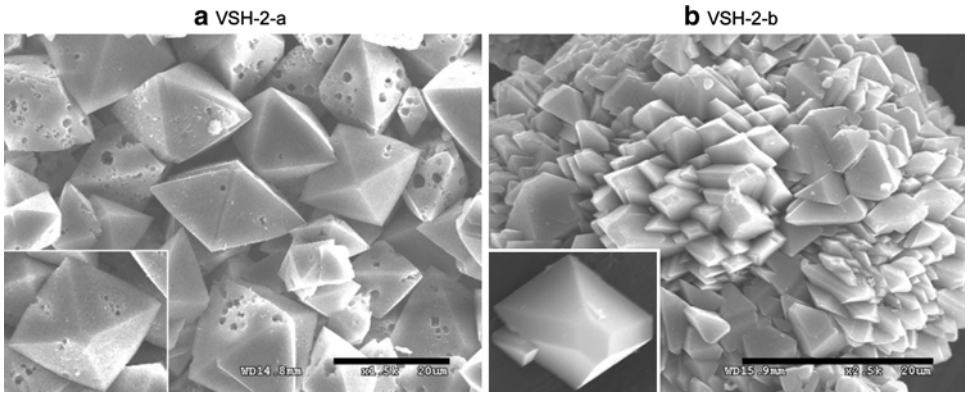

Fig. 3 SEM images of VSH-2-a and VSH-2-b. *Scale bars* = 20 μm

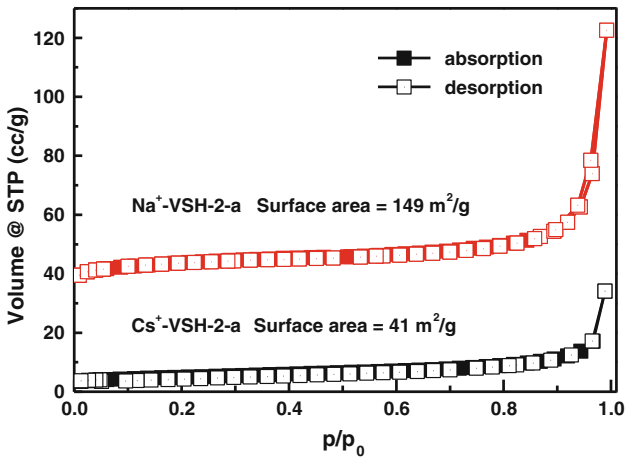

Fig. 5 N_2 absorption isotherms of Cs^+–VSH-2-a and Na^+–VSH-2-a

however, the absorption maximums in the UV region, that is, the 215, 250, and 313 nm bands, progressively red-shifted upon changing the cation from Cs^+ to Na^+, Ca^{2+}, and to Pb^{2+}. Since their Sanderson's electronegativities of the cations were 0.220, 0.560, 0.946, 1.900, respectively [12], the above phenomenon indicates that the absorption maximums in the UV region progressively red shift with increasing the Sanderson's electronegativities of the counter cations. Based on the well established facts that the framework oxygen atoms act as the electron donors and the counter cations act as the electron acceptors in the dehydrated state [9, 13, 14] and that the cations bind to the framework oxygen atoms upon dehydration, the above phenomenon is ascribed to unique charge-transfer (CT) interactions among the V^{4+}, O^{2-}, and M^{n+}, as illustrated in Fig. 7 [9].

Thus, in the dehydrated state (Fig. 7a), the interaction between the V^{4+} and O^{2-} is a metal-to-framework oxide charge-transfer (MFCT) interaction, in other words, a metal-to-ligand charge-transfer (MLCT) interaction and that between O^{2-} and M^{n+} is a framework oxide-to-counter cation charge-transfer (FCCT) interaction, in other words, a ligand-to-metal charge-transfer (LMCT) interaction. This reveals an unprecedented interesting situation that in the dehydrated VSH-2 the framework oxide plays the role of both acceptor and donor. In the hydrated state, the V^{4+} to O^{2-} MLCT interaction still remains while the O^{2-} to M^{n+} LMCT interaction disappears due the breakage of the direct CT interaction between the framework oxide and the counter cation owing to the hydration of the cation (Fig. 7b). As a result, the UV region spectra remain the same regardless of the type of the cation or the electronegativity of the cation (Fig. 6a, b).

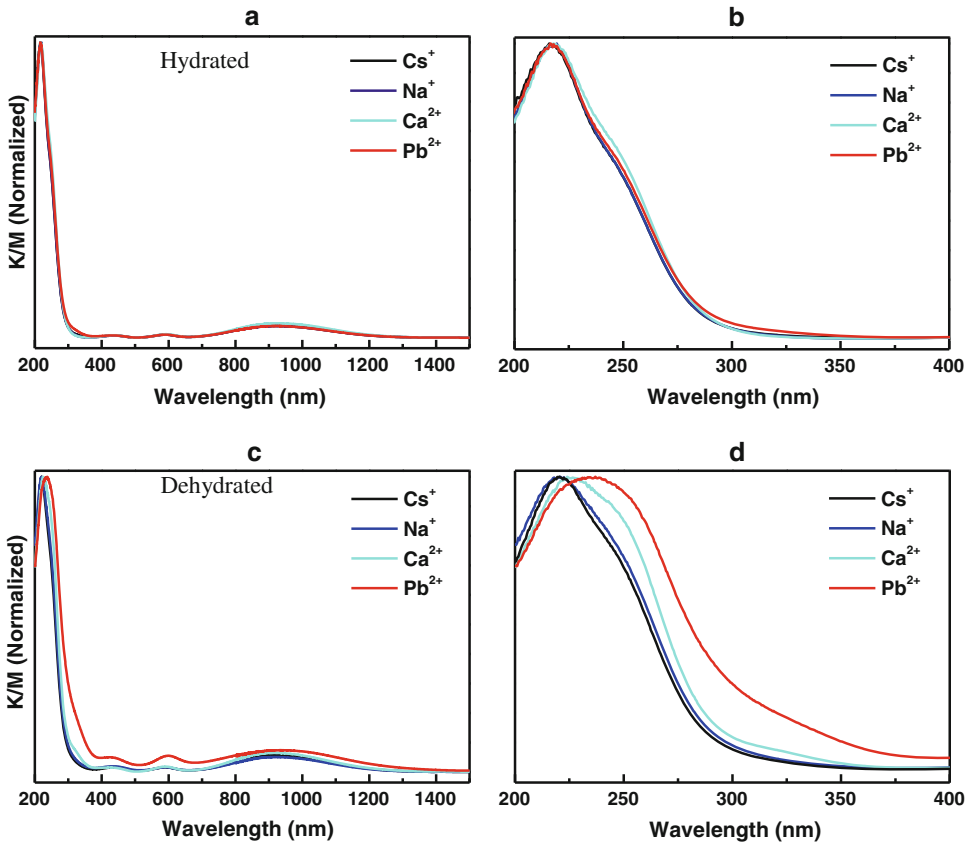

Fig. 6 Diffuse reflectance UV–Vis spectra of the hydrated (**a**, **b**) and dehydrated (**c**, **d**) M^{n+}–VSH-2-a, where M^{n+} = Cs^+, Na^+, Ca^{2+}, and Pb^{2+}, respectively, in two different wavelength ranges, 200–1500 (**a**, **c**) and 200–400 nm ranges (**b**, **d**). The progressive red shift of the spectrum upon changing M^{n+} from Cs^+ to Pb^{2+} shows the V^{4+}-to-O^{2-} charge-transfer interaction

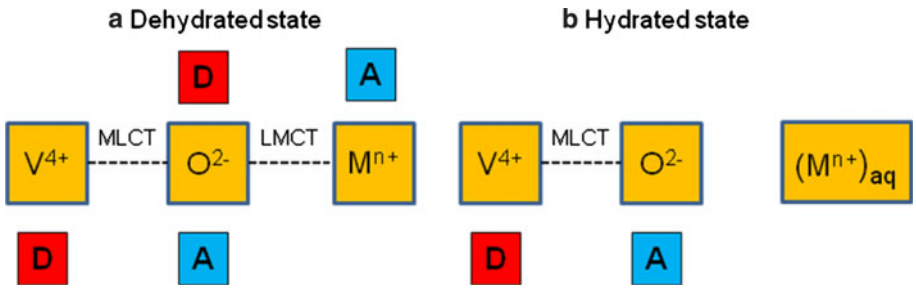

Fig. 7 Schematic illustrations showing the natures of interaction among V^{4+}, O^{2-}, and M^{n+} in VSH-2 in the dehydrated (**a**) and hydrated (**b**) states

The fact that the absorption maximums in the visible region, that is, the 437, 590, and 914 nm bands do not shift to the lower energy region indicates that they are not related to the MLCT or LMCT interaction. We therefore propose that the visible bands arise due to the d–d transition of V^{4+}. Similar conclusions were made from AM-6 [9].

3.6 Magnetic Susceptibility and ESR Spectra

The formula of VSH-2, $Cs_2(VO)(Si_6O_{14})\cdot 3H_2O$, indicates that the oxidation state of the vanadium atoms should be 4+. This means that each vanadium atom should have one unpaired electron, and hence the theoretical atomic magnetic moment (μ) should be 1.73 BM. The plot of the reciprocal magnetic susceptibility ($1/\chi_M$) with respect to the temperature (T) for VSH-2-a sample is shown in Fig. 8a. The slope (μ) of VSH-2-a was 1.64 BM. This result indicates that while most of the vanadium atoms in VSH-2 exist in the +4 oxidation state, small amounts of vanadium atoms exist in the +5 oxidation state. The ESR spectrum of VSH-2-a (Fig. 8b) showed a strong signal of V^{4+} with the g value of 1.959 with ΔH_{pp} value of 168 G, consistent with the presence of an unpaired electron in each V^{4+} ion. The above results show that despite the fact that V_2O_5 was used as the vanadium source the oxidation states of most of the vanadium atoms in the produced VSH-2 are 4+, as was observed during the synthesis of AM-6 using V_2O_5 as the vanadium source [9]. We believe that the added ethanol acts as a very effective reducing agent. We are currently investigating the effect of other alcohols on the morphology of VSH-2.

3.7 Raman Spectra

The Raman spectrum of the hydrated Cs^+–VSH-2-a in the 200–1400 cm^{-1} region (Fig. 9a) showed the presence of a strong V=O vibration band at 960 cm^{-1} together with small peaks at 382 (weak), 462 (weak), 540 (weak), 624 (medium), 800 (weak), and 1,080 (weak). Among these we propose that the 624 cm^{-1} band arises due to V–O–Si stretching, since a similar band appears from the AM-6. To investigate the effect of the cation on the V=O vibration band, we measured the Raman spectra of M^{n+} –VSH-2-a, (M^{n+} = Cs^+ Na^+, Ca^{2+}, and Pb^2) in the hydrated (Fig. 9b) and dehydrated (Fig. 9c) states. In the hydrated state, the V=O vibration band appeared at 960 cm^{-1} regardless of the type of cation. However, in the dehydrated state, the Raman band shifted to the higher energy region upon increasing the Sanderson's electronegativity of the counter cation. Thus, the V=O stretching band appeared at Cs^+: 960, Na^+: 963, Ca^{2+}: 984, and Pb^{2+}: 995 cm^{-1}. It is also noteworthy that the V=O stretching band becomes broad when M^{n+} is Pb^{2+}, indicating a strong interaction between the V=O group and Pb^{2+} in the dehydrated state.

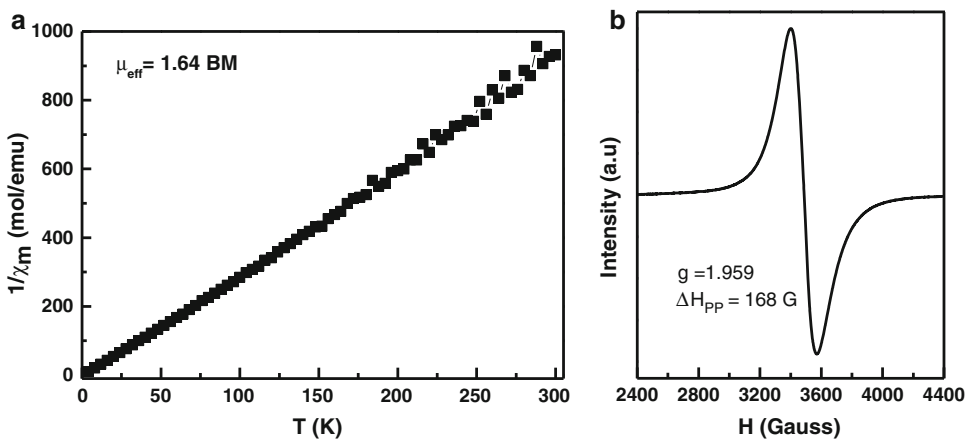

Fig. 8 **a** The plot of the reciprocal magnetic susceptibility ($1/\chi_M$) of Cs^+ –VSH-2-a with respect to the temperature (T). **b** ESR spectra of Cs^+–VSH-2-a obtained at room temperature

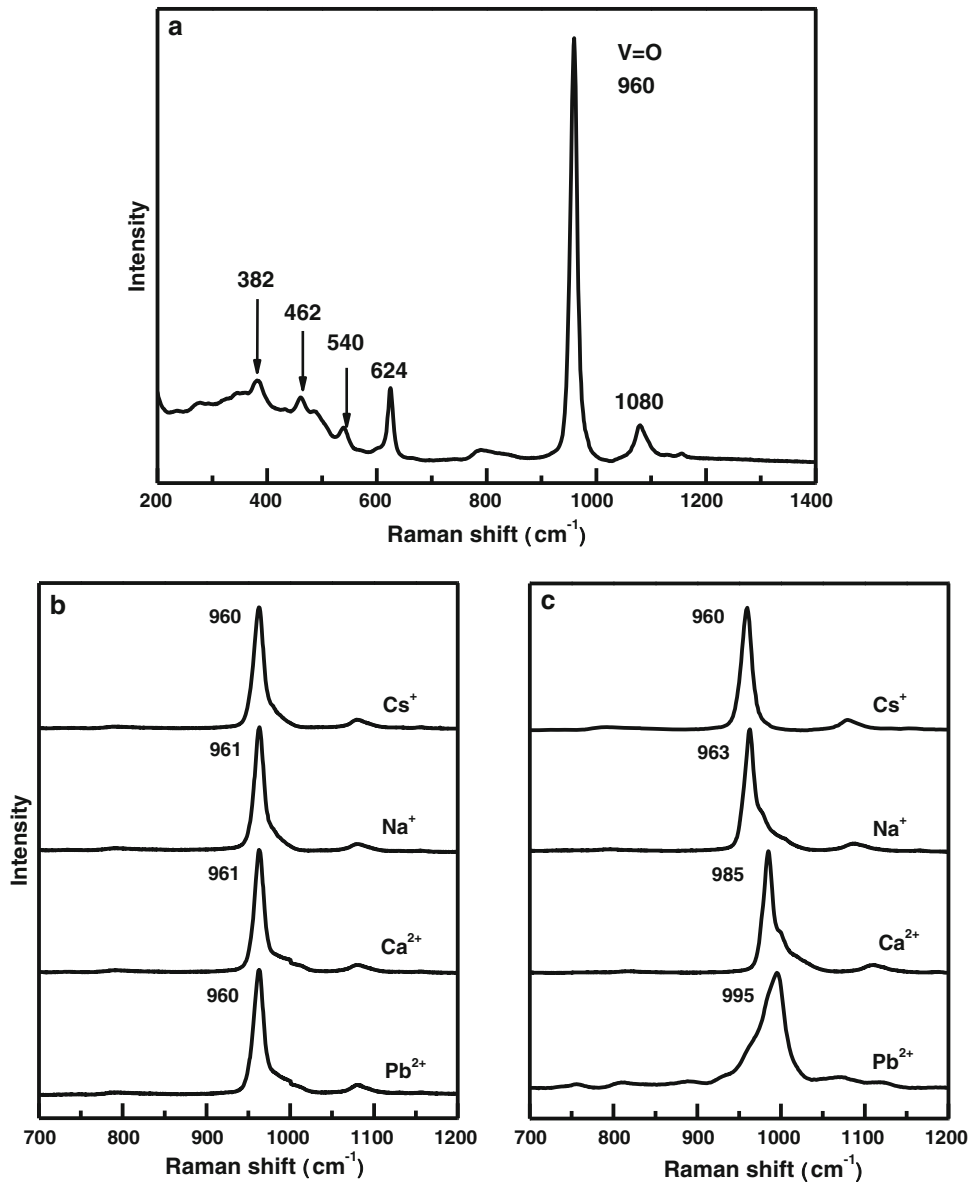

Fig. 9 Raman spectra of Cs^{+}–VSH-2-a (pristine) in the hydrated state in the 200–1400 cm^{-1} region (**a**) and M^{n+}–VSH-2-a in the hydrated (**b**) and dehydrated (**c**) states, where $M^{n+} = Cs^{+}$, Na^{+}, Ca^{2+}, and Pb^{2+} (as indicated) in the 700–1200 cm^{-1} region. **c** shows that the V=O stretching frequency shifts to the higher energy region upon dehydration and upon increasing the electronegativity of the cation

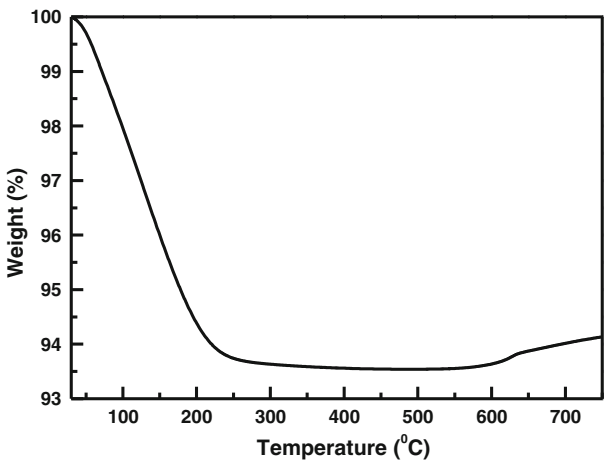

Fig. 10 TGA of VSH-2-a

3.8 Thermogravimetric Analysis (TGA)

A TGA analysis of VSH-2-a was conducted between the room temperature and 750 °C (Fig. 10). The gradual water loss took place until ~250 °C and at ~550 °C the weight increase due to the oxidation of V^{4+} to V^{5+}. This indicates that the VSH-2 is thermally stable up to 550 °C.

4 Conclusions and Remarks

VSH-2 has a potential to be used as various catalysts. However, there have been no methods to synthesize pure VSH-2 in large quantities. As a result, the catalytic activities of VSH-2 have not been investigated. This work demonstrates for the first time the method to synthesize

pure VSH-2 in large quantities. So we hope that our work provides an opportunity to elucidate the catalytic properties of VSH-2 and its other useful physicochemical properties. The most interesting feature of the synthetic procedure is that while V_2O_5 is used as the V source, the resulting VSH-2 contains mostly V^{4+}. This means that V^{5+} in V_2O_5 is reduced during the synthetic procedure. Interestingly, the added ethanol works as the reducing agent. A similar phenomenon was observed during the synthesis of AM-6 [9]. We believe that this novel "reductive synthesis approach" of transition metal silicates will allow synthesis of many novel transition metal silicates. Among various absorption bands, 215, 250, and 313 nm bands arise due to the V^{4+} to O^{2-} metal-to-ligand charge transfer (MLCT) and the 437, 590, and 914 nm bands arise due to the d-d transition of V^{4+}. The phenomenon of V^{4+}-to-framework oxide charge transfer or MLCT is interesting and has also been observed from AM-6 [9]. This is an interesting phenomenon which could be exploited for various applications. The observation of the gradual shift of the V=O stretching band to higher energy region upon increasing the electronegativity of the counter cation or decreasing the electron density from V=O unit is an interesting phenomenon which will help elucidate the nature of V=O bonding.

References

1. Wang X, Liu L, Jacobson AJ (2001) Angew Chem 113: 2232–2234
2. Wang X, Liu L, Jacobson AJ (2002) J Am Chem Soc 124:7812–7820
3. Li C-Y, Hsieh C-Y, Lin H-M, Kao H-M, Lii K-H (2002) Inorg Chem 41:4206–4210
4. Staples LW, Evans HT Jr, Lindsay JR (1973) Am Mineral 58:405–411
5. Evans HT Jr (1973) Am Mineral 58:412–424
6. Rocha J, Brandão P, Lin Z, Anderson MW, Alfredsson V, Terasaki O (1997) Angew Chem Int Ed 36:100–102
7. Ismail MN, Fraiman ND, Callahan DM Jr, Gursoy G, Viveiros E, Ozkanat O, Ji Z, Willey RJ, Warzywoda J, Sacco A Jr (2009) Microporous Mesoporous Mater 120:454–459
8. Yeates RM, Murdoch MJ, Southon PD, Mclaughlin AC, Howe RF, Bonino F, Bordiga S, Damin A (2009) Dalton Trans 38: 8025–8032
9. Datta SJ, Yoon KB (2010) Angew Chem Int Ed 49:4971–4975
10. Brandão P, Valente A, Philippou A, Ferreira A, Anderson MW, Rocha J (2003) Eur J Inorg Chem 6:1175–1180
11. Brandão P, Philippou A, Hanif N, Ribeiro-Claro P, Ferreira A, Anderson MW, Rocha J (2002) Chem Mater 14:1053–1057
12. Sanderson RT (1983) J Am Chem Soc 105:2259–2261
13. Park YS, Um SY, Yoon KB (1999) J Am Chem Soc 121: 3193–3200
14. Jeong NC, Lee YJ, Park J-H, Lim H, Shin C-H, Cheong H, Yoon KB (2009) J Am Chem Soc 131:13080–13092